ARTICLE

Probing Exciton Localization in Single-Walled Carbon Nanotubes Using High-Resolution Near-Field Microscopy

Carsten Georgi,[†] Alexander A. Green,[‡] Mark C. Hersam,[‡] and Achim Hartschuh[†,*]

[†]Department Chemie and CeNS, Ludwig-Maximilians-Universität München, 81377 München, Germany, and [‡]Department of Materials Science and Engineering, Department of Chemistry, Northwestern University, Evanston, Illinois 60208-3108

ABSTRACT We observe localization of excitons in semiconducting single-walled carbon nanotubes at room temperature using high-resolution near-field photoluminescence (PL) microscopy. Localization is the result of spatially confined exciton energy minima with depths of more than 15 meV connected to lateral energy gradients exceeding 2 meV/nm as evidenced by energy-resolved PL imaging. Simulations of exciton diffusion in the presence of energy variations support this interpretation predicting strongly enhanced PL at local energy minima.

KEYWORDS: single-walled carbon nanotubes · photoluminescence · excitons · localization · near-field microscopy

Owing to the exceptional optical properties of carbon nanotubes, their application in optoelectronics, nanoelectronics, and biosensing is widely investigated and expected to be of major importance in future nanoscale technology.[1,2] Optical excitation of semiconducting single-walled carbon nanotubes (SWNTs) generates excitons with binding energies of several hundreds of meV dominating virtually all optical phenomena, such as absorption and photoluminescence (PL).[3] Exciton decay is dominated by nonradiative processes with rather short lifetimes in the range of few tens of picoseconds, further reduced by exciton−exciton annihilation at higher excitation levels.[4−8] Exciton energies and decay dynamics have been investigated extensively on the single nanotube level using diffraction-limited confocal PL microscopy. Near-field optical microscopy circumvents this limit and offers the possibility to study nanotube properties on the nanoscale, revealing for example, local structural variations or localized quenching sites.[9−11]

Exciton localization can occur in SWNTs due to potential energy fluctuations along the nanotube. In fact, the quasi-1D, single atomic layer structure of SWNTs makes them particularly sensitive to external perturbations caused by, for example, variations in the local dielectric function, trapped charges, or adsorbed species. In freely suspended SWNTs excitons are highly mobile with diffusion lengths up to 600 nm, whereas for SWNTs on substrates the mobility is significantly reduced to an average value of about 100 nm due to environmental coupling.[11−16]

The localization of intrinsically mobile excitons strongly affects the optical properties of SWNTs and will be relevant for applications relying on energy transfer such as excitonic solar cells.[17] Localized excitons show increased exciton−phonon coupling and are thus subject to faster phonon-induced nonradiative loss channels.[18] The inhomogeneous exciton distribution that arises from localization will affect the exciton−exciton annihilation dynamics and the PL saturation behavior at increased excitation levels. Additionally, quantum emission in terms of photon-antibunching has been attributed to strong localization combined with efficient exciton−exciton annihilation which inhibits simultaneous emission.[19,20] SWNTs could thus be used as single photon sources with spatially confined emission sites in novel nanophotonic devices that could also be driven electrically.

Exciton localization has been observed at low temperatures where its spectral and temporal characteristics become apparent in diffraction-limited PL experiments.[19−22] To date all observations on exciton localization were indirect in the sense that the spatially confined distribution of excitons was not probed by direct imaging. The relevant length scales below 100 nm are not accessible by conventional diffraction-limited confocal microscopy. In this work we applied tip-enhanced near-field optical microscopy (TENOM)[23] as a tool to visual-

*Address correspondence to achim.hartschuh@cup.uni-muenchen.de.

Received for review June 25, 2010 and accepted September 8, 2010.

Published online September 21, 2010. 10.1021/nn101443d

© 2010 American Chemical Society

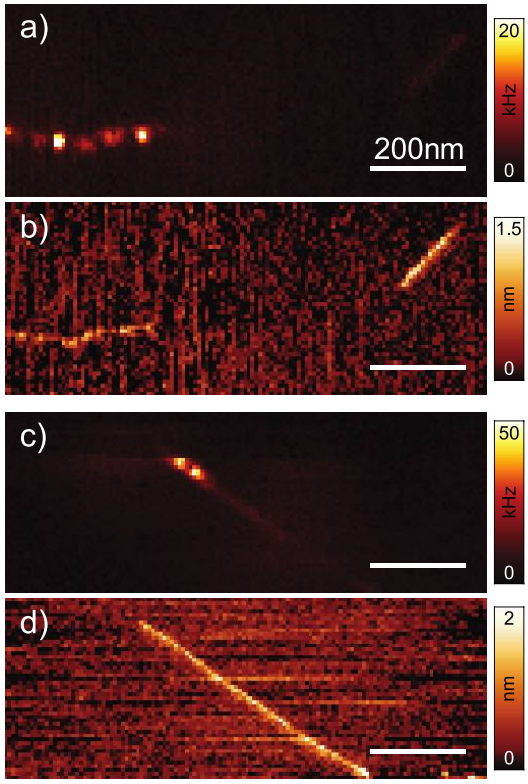

Figure 1. Near-field PL images of SWNTs showing strongly localized and bright PL. (a and c) Near-field PL intensity (photon count rates); (b and d) corresponding topography image. The scale bar is 200 nm for all images. The strong PL in these cases is localized within regions smaller than 30 nm, which cannot be explained by quenching defects in between at similar distances. Such closely spaced defects would quench nearly all PL due to exciton mobility. We attribute the strong PL at these spots to an increased exciton density due to localization.

ize exciton localization at room temperature by imaging the PL intensity and energy along SWNTs with a spatial resolution of about 15 nm. We find that spatially confined exciton energy minima with depths of about 15 meV connected to lateral energy gradients in the order of 2 meV/nm induce localization resulting in locally very bright PL. Numerical simulations of near-field PL data in the presence of directed exciton diffusion support our discussion.

RESULTS AND DISCUSSION

We investigate the local PL properties of DNA-wrapped semiconducting SWNTs on a mica substrate using TENOM. A common observation is that the PL intensity along the nanotube is highly nonuniform on the nanoscale. This can in part be attributed to randomly distributed defects that quench the excitons in their vicinity, leading to a strong PL reduction on a length of about 100 nm due to exciton mobility.[11] For about 5−10% of the investigated nanotubes, we observe very localized PL emission spots which appear very bright and are unlikely to be caused by quenching defects. Two examples are shown in Figure 1, where bright PL spots are localized within 30 nm. Assuming quenching sites in between these spots as origin of the PL variations, we would expect that the PL almost vanishes. For quenching sites with distances below 50 nm, most of the excitons generated in between will certainly reach the defects due to their mobility and thus get quenched.

We believe that the localized bright PL originates from an increased exciton density due to exciton localization in terms of trapping. We know from earlier experiments that DNA-wrapping can be nonuniform along the nanotubes and can locally decrease the exciton energy.[9] If the effect occurs very localized and exciton energy gradients along the nanotube become large enough, this could affect the exciton diffusion and lead to an increased exciton density at these local exciton energy minima. The bright and localized PL emanating from these minima will in turn be lower in energy, that is, red-shifted. In the following we used near-field spectroscopic imaging to map the emission energy with nanoscale resolution.

Figure 2 panels a and b show a near-field PL image of several luminescent SWNTs and the corresponding topography. The short nanotube in the upper part is much brighter than the other present SWNTs with strong PL intensity variations on length scales of about 10 nm. In particular, the strongest PL intensity with photon count rates above 100 kHz is emitted very locally in the upper part of this nanotube. This unusual bright and localized PL indicates exciton localization which is supported by the subsequent spectroscopic image from the marked area in Figure 2a. Here, a complete spectrum was recorded at each pixel to determine the local PL energy. The results are depicted in Figure 2c,d, showing PL intensity and energy derived from peak fitting the spectra at each image pixel. Along the 160 nm long SWNT, the PL energy varies by about 30 meV. For the upper and lower nanotube section this correlates well with bright PL at energy minima (see also Figure 2f). The PL in the middle section is very weak, which we attribute to a quenching defect at this position. During the preceding near-field scan on this SWNT (Figure 2a), this section still appeared bright. However, also traces of PL blinking were seen, which is a sign for the formation of photoinduced defects.[14] We assume that the first scan induced a defect which quenches the PL in the middle section of the nanotube. Although nanotube PL is found to be remarkably stable during image scans taking up to 30 min, additional quenching sites are sometimes introduced and need to be considered in the data analysis.

The correlation between PL intensity and energy is displayed in Figure 2e, using data from all image pixels (open and closed squares). Clearly, bright PL is associated with lower energy and higher energy emission is weak as expected for energy induced localization. For two reasons we do not expect an exclusive correlation between PL intensity and energy. First, the imaging pro-

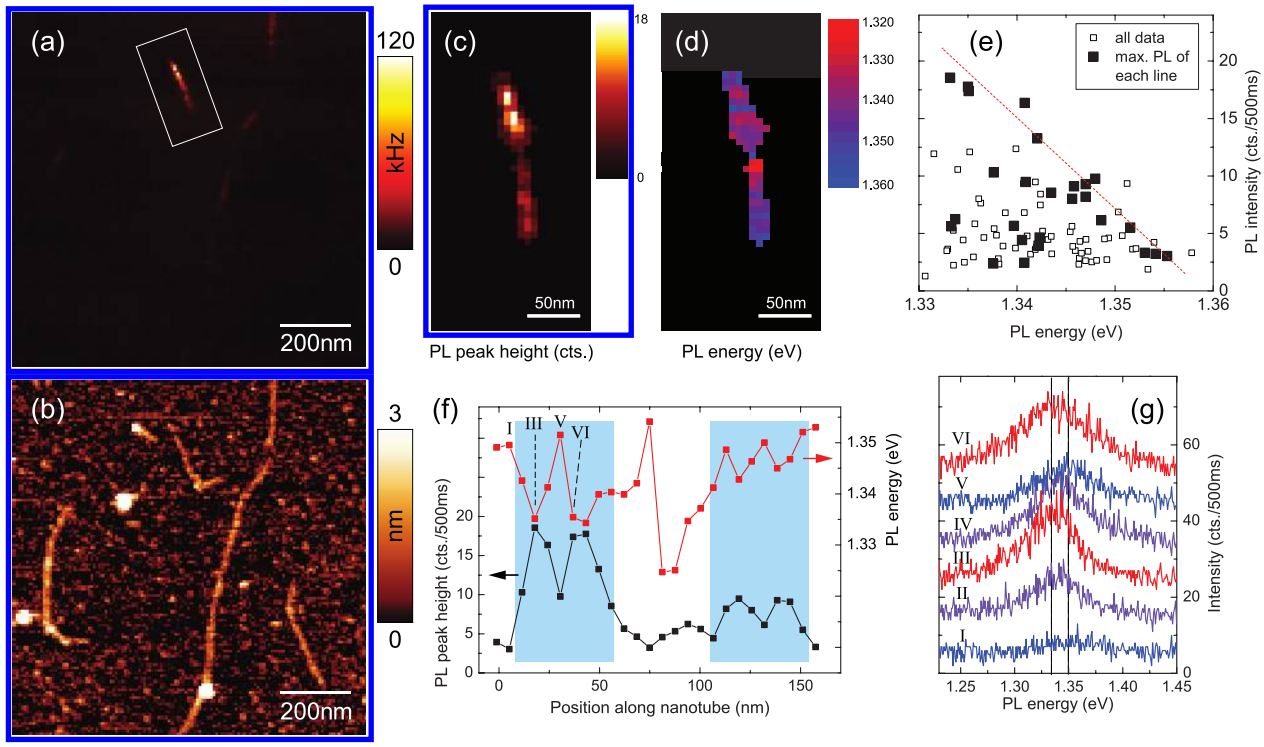

Figure 2. Exciton localization in a 160 nm long (9,1) SWNT. (a and b): Near-field PL image and corresponding topography showing several luminescent nanotubes. The very bright nanotube with strong local PL variations indicates exciton localization. (c and d): Maps of the PL intensity and energy derived from a subsequent spectroscopic image of the area marked in panel a by peak fitting the recorded spectra at each image pixel. (e) Correlation between PL intensity and energy for all image pixels (open squares), with the brightest pixel of each image line being highlighted (filled squares) to account for the influence of finite spatial resolution (see text). (f) PL intensity and energy plotted along the nanotube. In the upper and lower section of the nanotube (shaded area), bright PL is clearly correlated with lower energy. Weak PL in the middle section is attributed to additional quenching defects (see text). (g) Near-field spectra from six adjacent positions (I−VI) along the nanotube, equally spaced by 6.5 nm and marked in panel e. The PL energy shifts by up to 15 meV (range indicated by the two dashed lines) between two neighboring positions. These strong exciton energy gradient of ~2 meV/nm in the configuration of a potential minimum lead to exciton localization.

cess with its finite point spread function results in many data points below the dashed line. In the present image we used a pixel size of 6.5 nm which is about three times smaller than the optical resolution. Hence, there are always several pixels with lower intensity surrounding a central pixel with maximum tip enhancement, all at the same PL energy. By selecting only the brightest pixel of each image line across the nanotube (closed squares in panel e), this effect is avoided at least in one direction, and the correlation becomes much clearer, since most of the omitted pixels are below the line. Second, exciton localization is not the only factor determining the PL intensity. Local defects and doping will quench excitons and thus reduce PL intensity.

In Figure 2f, PL intensity and energy are plotted against the position along the nanotube. In the upper part of the SWNT, where the relation between strong PL and low energy is most pronounced, the energy varies on very small length scales. The pronounced energy minimum between positions I and V has a depth of about 15 meV and extends only 25 nm. The corresponding energy gradients toward the minimum are about 1.2 meV/nm, which creates an efficient driving force for exciton drift. The neighboring positions V and VI have an energy difference of 15 meV at a distance of only 6.5 nm, corresponding to a gradient exceeding 2 meV/nm. Due to the finite optical resolution the actual gradient in the nanotube is expected to be even larger. In the middle section a PL energy drop of even 30 meV/6.5 nm (~5 meV/nm) can be seen, though due to the weak PL intensity this value is not as reliable. Figure 2g shows the corresponding PL spectra from positions I−VI with clearly visible peak-shifts on very small length scales. It becomes clear that for efficient exciton localization, the exciton energy minima must be sufficiently deep and spatially confined.

Figure 3a illustrates localized and strong PL for another nanotube. The simultaneously recorded topography (Figure 3b) demonstrates that the nanotube is about 450 nm long. However, PL is only emitted from three points in the left part of the SWNT. The PL intensity and energy exhibit the same correlation as presented in Figure 2e (see Figure S2 in the Supporting Information). Based on the PL energy, the chirality of the SWNT is assigned as (9,1). Compared to the average PL energy of DNA-wrapped (9,1)-SWNTs on substrate of 1.332 eV, the localized PL observed in Figure 3d with energies down to 1.310 eV is exceptionally red-shifted.[9] This can account for the strong degree of localization in Figure 3a.

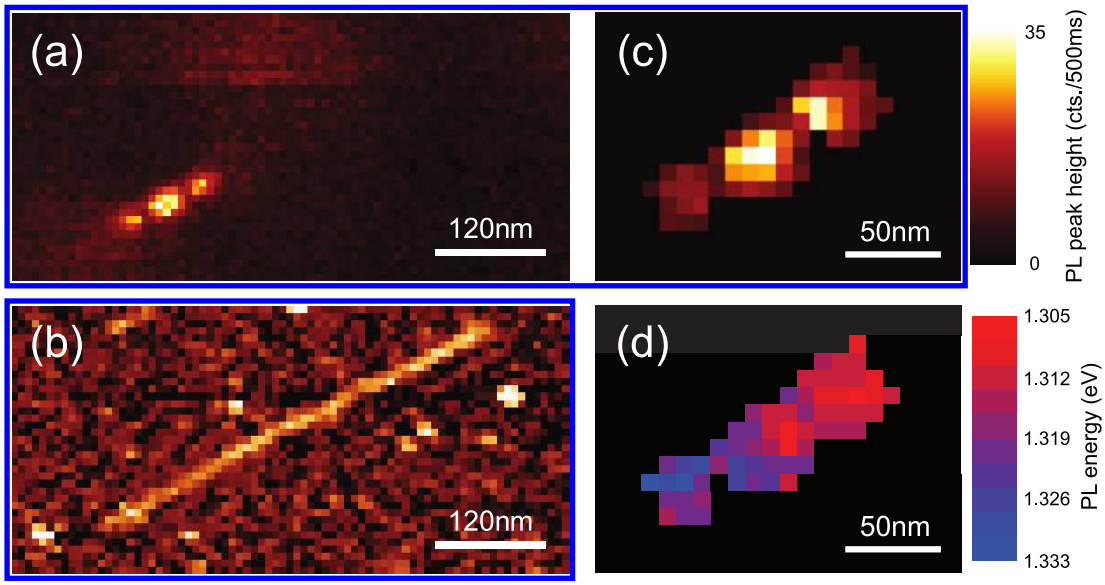

Figure 3. Near-field PL (a) and topography image (b) of a 450 nm long (9,1) SWNT. Maps of the PL intensity (c) and energy (d) derived from a subsequent spectroscopic image. Bright PL is apparently shifted to lower energy.

To support our model of exciton diffusion and localization, we complemented our experiment with numerical simulations. Here, the evolution of exciton population is described by 1D-diffusion according to Fick's Second Law, including exciton decay. Since the exciton size of 1−2 nm is much smaller than the discussed length scales as, for example, diffusion length or spatial resolution, and the exciton binding energy is one order of magnitude larger than the observed energy variations, the exciton can be treated as a single point-like object.[24] For flexible numerical treatment, the 1D-diffusion is reproduced by the 1D random walk with discretized time and position along the nanotube. During each time step Δt the exciton diffuses $\pm\Delta x$ with equal probability in the case of uniform exciton energy. The exciton population N_x^t at each time t and position x is calculated by

$$N_x^t = \frac{1}{2}(N_{x-\Delta x}^{t-\Delta t} + N_{x+\Delta x}^{t-\Delta t}) - \frac{\Delta t}{\tau}N_x^{t-\Delta t} \qquad (1)$$

Choosing an appropriate value for Δx, the term $\Delta t/\tau$ which accounts for the exciton decay is given by $\Delta t/\tau = (\Delta x/L)^2$, with the diffusion length $L = 100$ nm.[11−14] The exciton lifetime τ itself does not have to be defined in the simulation, it is contained within the diffusion length L. Changes of the radiative and nonradiative decay rates in the vicinity of the gold tip are expressed as relative changes of the exciton lifetime. Exciton−exciton annihilation is neglected since excitation intensities are low and only one exciton is present at a time. We can therefore calculate the time-integrated exciton population over all timesteps until complete decay to account for the continuous excitation and time-integrated detection in the experiment. Without exciton−exciton interactions, the time-integrated probability distribution for one excitation cycle is equivalent to the solution of a steady-state ansatz used in other publications (see also Supporting Information).[13,16]

For nonuniform exciton energy E_{exc} along the SWNT arising from an inhomogeneous environment, we expect a different branching ratio with higher probability of diffusion toward lower energy. We introduce the probabilities $\vec{p}_x$ and $\overleftarrow{p}_x$ with $\vec{p}_x + \overleftarrow{p}_x = 1$, which describe the fraction of exciton population at position x transferring to left or right, respectively. Since the diffusion is temperature driven, the ratio of both probabilities is given by the Boltzmann factor

$$\vec{p}_x/\overleftarrow{p}_x = \exp(-\Delta E_x/kT) \qquad (2)$$

with ΔE_x being the exciton energy difference between the right and left vicinity of position x. Using these definitions, the exciton population is then calculated by

$$N_x^t = \vec{p}_{x-\Delta x}N_{x-\Delta x}^{t-\Delta t} + \overleftarrow{p}_{x+\Delta x}N_{x+\Delta x}^{t-\Delta t} - \frac{\Delta t}{\tau}N_x^{t-\Delta t} \qquad (3)$$

In the Supporting Information we show that our approach of modified branching ratios corresponds to the Fokker−Planck equation, which adds a drift term to Fick's Law of diffusion. This drift term is related to the local exciton energy gradients. Figure 4a illustrates the numerical calculation of directed exciton diffusion due to spatial exciton energy variations. The exciton population, represented by bars, is predicted to increase at the energy minima because of enhanced diffusion toward lower energy. To connect the resulting simulated exciton distributions and experimental data, we have reproduced the complete TENOM imaging process and simulated the detected near-field PL intensity along nanotubes (see Methods section and Supporting Information for details).

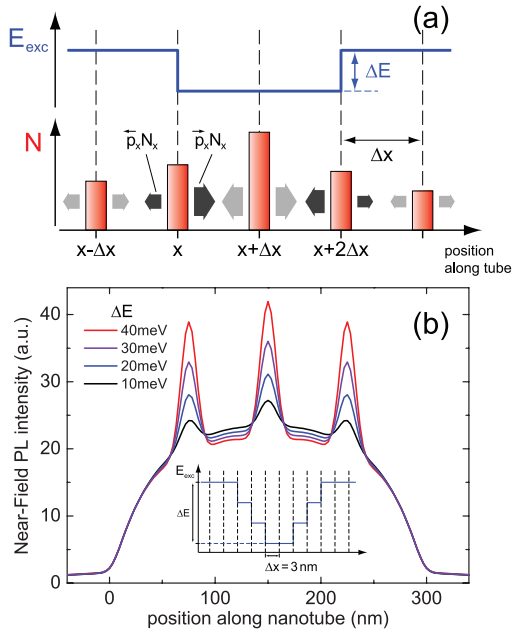

Figure 4. (a) Schematic illustrating the numerical calculation of exciton diffusion. At each discrete position along the nanotube (x, $x + \Delta x$,) the local exciton population N is represented by a bar. The nonuniform exciton energy E_{exc} is shown above. At each simulation time step, the population at a position is transferred to its left and right neighbor according to eq 2, indicated by broad arrows. (b) Simulated near-field PL intensity for a 300 nm long carbon nanotube. Three exciton energy minima have been introduced to the nanotube, centered at 75, 150, and 225 nm from the left nanotube end. The profile of the energy minima is shown in the inset, the depth ΔE is varied between 10 and 40 meV. Because of enhanced exciton diffusion toward energy minima, the PL intensity is increased at these positions.

Figure 4b shows calculated PL intensity profiles along a 300 nm long nanotube with three energy minima of depth ΔE, varied between 10 and 40 meV on a length scale of about 10 nm (see inset). The calculations indicate that for exciton energy minima with depths above 10 meV, the localization effect becomes significant and clearly observable with TENOM. This corresponds to exciton energy gradients in the order of several meV/nm, in good agreement with the presented experiments. Our simulations thus strongly support the model of energy-induced exciton localization. The model also shows, that at low temperature the influence of energy gradients on exciton diffusion according to eq 2 is remarkably increased. Localization is then expected to be far more efficient and will dominate the PL properties even in confocal experiments. This is supported by the observation of quantum emission in terms of photon antibunching below 25 K.[19,20] For a confocal PL measurement at room temperature however, exciton localization will only lead to spectral broadening due to spatial averaging.

The observed exciton energy variations can arise from dielectric screening, determined here by the dielectric constants of DNA and substrate, doping related screening, and the Stark effect due to localized charges in the vicinity of the nanotube creating strong local fields.[21,25−28] Since DNA features a negatively charged backbone, its presence can induce PL energy variations *via* all three mechanisms. The observed spatial PL energy variations can thus be attributed mainly to the heterogeneous environment resulting from nonuniform DNA-wrapping. Local changes of the PL energy caused by DNA-wrapping have been observed previously with TENOM, however without indication of exciton localization due to much smaller exciton energy gradients in the order of 0.2 meV/nm.[9] Assuming randomly distributed DNA-strands, a configuration forming isolated and deep potential minima is expected to occur rarely. This can explain why we observe pronounced exciton localization only in 5−10% of the near-field PL images.

Localized PL emission in a SWNT has been observed previously with TENOM near a negatively charged defect connected to characteristic Raman scattering signals.[10] In this case, PL occurred at a single position only, inhibiting energy-resolved imaging and the investigation of energy induced localization. Since we only detected very weak Raman scattering for the present nanotube material, a corresponding signal analysis regarding defects and defect type was not possible.

CONCLUSIONS

We observed the localization of excitons in semiconducting single-walled carbon nanotubes at room temperature as a result of spatially confined exciton energy minima with depths of 15 meV and lateral energy gradients exceeding 2 meV/nm. Simulations based on a 1D random walk and accounting for the near-field imaging process support this interpretation predicting strongly enhanced exciton populations at localized energy minima. Directional or limited diffusion affects all physical phenomena that are connected to exciton mobility such as exciton−exciton annihilation and quenching by local defects.

METHODS

Experimental Setup. The tip-enhanced near-field optical microscope (TENOM) combines an inverted confocal microscope with a shear force mechanism to position a sharp gold tip in the center of the laser focus about 2 nm above the sample surface. Strongly enhanced excitation and radiation rates confined to the vicinity of the tip allow for the local imaging of the optical properties of the SWNT. The optical signal at each image pixel is detected either by a spectrograph and CCD or by an avalanche photodiode (APD) after spectral filtering. The incident laser power for PL imaging is kept low (~10 μW) to minimize photo-induced PL bleaching.[14]

Materials. The nanotubes studied in this work were semiconducting CoMoCAT-SWNTs wrapped by $(GT)_{10}$ single-stranded

DNA in aqueous solution.[29] The solution was spun onto a freshly cleaved thin layer of mica glued on a glass cover slide, providing an atomically smooth surface (additional details in Supporting Information). The DNA-wrapping is used to provide individual nanotubes with a well-defined topography on the sample surface. Standard surfactants such as sodium cholate which can also be used to disperse SWNTs in aqueous solution usually form a nonuniform film on the sample. This strongly affects the TENOM measurements by modulating the tip−sample distance and thus the near-field enhancement. Quantitative signal analysis along SWNTs would not be possible.

Details of the Numerical Simulation. For comparison with near-field experiments, these images have to be simulated including both nanotube excitation and PL detection in presence of the tip. The initial population N_x^0 is determined by the excitation intensity along the nanotube, which is the intensity distribution of the confocal laser focus plus tip-enhanced excitation in its center. Due to efficient quenching expected at the nanotube ends, the exciton population is constantly set to zero at these positions.[11] Corresponding to the experimental procedure, the center of the laser focus is scanned along the nanotube. For each position of tip and laser with respect to the nanotube, the evolution of the exciton population and resulting PL are calculated. The radiative and nonradiative decay rates k_{rad} and k_{nr} are both enhanced in vicinity of the tip and thus position dependent. Efficient PL emission *via* the tip dipole increases k_{rad} and additional quenching at very close tip−sample distances due to the metal tip affects k_{nr}.[23,30,31] For SWNTs with a low quantum yield of $\sim 10^{-3}$, k_{rad} can be strongly increased, whereas additional quenching is insignificant. The PL emitted from a single point of the nanotube at each time step is given by $Q(x)\Delta t/\tau N_x^t$. $Q(x)$ is the quantum yield which is increased underneath the tip due to radiative rate enhancement. The measured PL in the cw-experiment is then calculated by summing over all timesteps until $t = 2\tau$ and along the whole nanotube, with τ being the exciton lifetime. The enhancement factors for excitation and radiative rate in vicinity of the tip (within 15 nm) are 25 and 10, respectively. The resulting signal enhancement is in agreement with the observed imaging contrast. The radiative rate enhancement is chosen to be smaller due to the weaker plasmonic response of our gold tips at the PL energy with respect to the excitation at 632.8 nm.[32]

Acknowledgment. This work was funded by the Deutsche Forschungsgemeinschaft (DFG-HA4405/3-1, DFG-HA4405/4-1 and the Nanosystems Initiative Munich (NIM)), the National Science Foundation (DMR-0520513, EEC-0647560 and DMR-0706067), and the Nanoelectronics Research Initiative.

Supporting Information Available: Details regarding sample preparation including the absorption spectrum of the SWNT solution; details on the simulation of exciton diffusion and the relation of diffusion constant, diffusion length and exciton lifetime; and the correlation of PL intensity and energy for the data set in Figure 3. This material is available free of charge *via* the Internet at http://pubs.acs.org.

REFERENCES AND NOTES

1. *Carbon Nanotubes*; Jorio, A., Dresselhaus, M. S., Dresselhaus, G., Eds.; Springer: Berlin/Heidelberg, 2008; Vol. 111.
2. Avouris, P.; Freitag, M.; Perebeinos, V. Carbon-Nanotube Photonics and Optoelectronics. *Nat. Photon.* **2008**, *2*, 341–350.
3. Wang, F.; Dukovic, G.; Brus, L. E.; Heinz, T. F. The Optical Resonances in Carbon Nanotubes Arise From Excitons. *Science* **2005**, *308*, 838–841.
4. Hagen, A.; Steiner, M.; Raschke, M. B.; Lienau, C.; Hertel, T.; Qian, H.; Meixner, A. J.; Hartschuh, A. Exponential Decay Lifetimes of Excitons in Individual Single-Walled Carbon Nanotubes. *Phys. Rev. Lett.* **2005**, *95*, 197401.
5. Wang, F.; Dukovic, G.; Brus, L. E.; Heinz, T. F. Time-Resolved Fluorescence of Carbon Nanotubes and Its Implication For Radiative Lifetimes. *Phys. Rev. Lett.* **2004**, *92*, 177401.
6. Gokus, T.; Hartschuh, A.; Harutyunyan, H.; Allegrini, M.; Hennrich, F.; Kappes, M.; Green, A. A.; Hersam, M. C.; Araujo, P. T.; Jorio, A. Exciton Decay Dynamics in Individual Carbon Nanotubes at Room Temperature. *Appl. Phys. Lett.* **2008**, *92*, 153116.
7. Berciaud, S.; Cognet, L.; Lounis, B. Luminescence Decay and the Absorption Cross Section of Individual Single-Walled Carbon Nanotubes. *Phys. Rev. Lett.* **2008**, *101*, 077402.
8. Ma, Y. Z.; Valkunas, L.; Dexheimer, S. L.; Bachilo, S. M.; Fleming, G. Femtosecond Spectroscopy of Optical Excitations in Single-Walled Carbon Nanotubes: Evidence for Exciton−Exciton Annihilation. *Phys. Rev. Lett.* **2005**, *94*, 157402.
9. Qian, H.; Araujo, P. T.; Georgi, C.; Gokus, T.; Hartmann, N.; Green, A. A.; Jorio, A.; Hersam, M. C.; Novotny, L.; Hartschuh, A. Visualizing the Local Optical Response of Semiconducting Carbon Nanotubes to DNA-Wrapping. *Nano Lett.* **2008**, *8*, 2706–2711.
10. Maciel, I. O.; Anderson, N.; Pimenta, M. A.; Hartschuh, A.; Qian, H.; Terrones, M.; Terrones, H.; Campos-Delgado, J.; Rao, A. M.; Novotny, L.; *et al*. Electron and Phonon Renormalization at Defect/Doping Sites in Carbon Nanotubes. *Nat. Mater.* **2008**, *7*, 878–883.
11. Georgi, C.; Böhmler, M.; Qian, H.; Novotny, L.; Hartschuh, A. Probing Exciton Propagation and Quenching in Carbon Nanotubes with Near-Field Optical Microscopy. *Phys. Stat. Sol. B* **2009**, *246*, 1460.1463.
12. Cognet, L.; Tysboulski, D. T.; Rocha, J.-D. R.; Doyle, C. D.; Tour, J. M.; Weisman, R. B. Stepwise Quenching of Exciton Fluorescence in Carbon Nanotubes by Single-Molecule Reactions. *Science* **2007**, *316*, 1465–1468.
13. Siitonen, A. T.; Tsyboulski, D. A.; Bachilo, S. M.; Weisman, R. B. Surfactant-Dependent Exciton Mobility in Single-Walled Carbon Nanotubes Studied by Single-Molecule Reactions. *Nano Lett.* **2010**, *10*, 1595–1599.
14. Georgi, C.; Hartmann, N.; Gokus, T.; Green, A. A.; Hersam, M. C.; Hartschuh, A. Photoinduced Luminescence Blinking and Bleaching in Individual Single-Walled Carbon Nanotubes. *ChemPhysChem* **2008**, *9*, 1460–1463.
15. Yoshikawa, K.; Matsuda, K.; Kanemitsu, Y. Exciton Transport in Suspended Single Carbon Nanotubes Studied by Photoluminescence Imaging Spectroscopy. *J. Phys. Chem. C* **2010**, *114*, 4353–4356.
16. Moritsubo, S.; Murai, T.; Shimada, T.; Murakami, Y.; Chiashi, S.; Maruyama, S.; Kato, Y. K. Exciton Diffusion in Air-Suspended Single-Walled Carbon Nanotubes. *Phys. Rev. Lett.* **2010**, *104*, 247402.
17. Gregg, B. A. Excitonic Solar Cells. *J. Phys. Chem. B* **2003**, *107*, 4688–4698.
18. Perebeinos, V.; Avouris, P. Phonon and Electronic Nonradiative Decay Mechanisms of Excitons in Carbon Nanotubes. *Phys. Rev. Lett.* **2008**, *101*, 057401.
19. Högele, A.; Galland, C.; Winger, M.; Imamoğlu, A. Photon Antibunching in the Photoluminescence Spectra of a Single Carbon Nanotube. *Phys. Rev. Lett.* **2008**, *100*, 217401.
20. Galland, C.; Högele, A.; Türeci, H. E.; Imamoğlu, A. Non-Markovian Decoherence of Localized Nanotube Excitons by Acoustic Phonons. *Phys. Rev. Lett.* **2008**, *101*, 067402.
21. Htoon, H.; O'Connell, M. J.; Cox, P. J.; Doorn, S. K.; Klimov, V. I. Low Temperature Emission Spectra of Individual Single-Walled Carbon Nanotubes: Multiplicity of Subspecies within Single-Species Nanotube-Ensembles. *Phys. Rev. Lett.* **2004**, *93*, 027401.
22. Hirori, H.; Matsuda, K.; Miyauchi, Y.; Maruyama, S.; Kanemitsu, Y. Exciton Localization of Single-Walled Carbon Nanotubes Revealed by Femtosecond Excitation Correlation Spectroscopy. *Phys. Rev. Lett.* **2006**, *97*, 257401.
23. Hartschuh, A. Tip-Enhanced Near-Field Optical Microscopy. *Angew. Chem., Int. Ed.* **2008**, *47*, 8178–8198.
24. Capaz, R. B.; Spataru, C. D.; Ismail-Beigi, S.; Louie, S. G. Diameter and Chirality Dependence of Exciton Properties in Carbon Nanotubes. *Phys. Rev. B* **2006**, *74*, 121401(R).

25. Walsh, A. G.; Vamivakas, A. N.; Yin, Y.; Cronin, S. B.; Ünlü, M. S.; Goldberg, B. B.; Swan, A. K. Scaling of Exciton Binding Energy with External Dielectric Function in Carbon Nanotubes. *Phys. E* **2007**, *40*, 2375–2379.
26. Freitag, M.; Steiner, M.; Naumov, A.; Small, J. P.; Bol, A. A.; Perebeinos, V.; Avouris, P. Carbon Nanotube Photo- and Electroluminescence in Longitudinal Electric Fields. *ACS Nano* **2009**, *3*, 3744–3748.
27. Matsuda, K.; Inoue, T.; Murakami, Y.; Maruyama, S.; Kanemitsu, Y. Exciton Fine Structure in a Single Carbon Nanotube Revealed Through Spectral Diffusion. *Phys. Rev. B* **2008**, *77*, 193405.
28. Perebeinos, V.; Avouris, P. Exciton Ionization, Franz−Keldysh, and Stark Effects in Carbon Nanotubes. *Nano Lett.* **2007**, *7*, 609–613.
29. Zheng, M.; Jagota, A.; Semke, E. D.; Diner, B. A.; Mclean, R. S.; Lustig, S. R.; Richardson, R. E.; Tassi, N. G. DNA-Assisted Dispersion and Separation of Carbon Nanotubes. *Nat. Mater.* **2003**, *2*, 338–342.
30. Anger, P.; Bharadwaj, P.; Novotny, L. Enhancement and Quenching of Single Molecule Fluorescence. *Phys. Rev. Lett.* **2006**, *96*, 113002.
31. Hartschuh, A.; Qian, H.; Meixner, A. J.; Anderson, N.; Novotny, L. Nanoscale Optical Imaging of Excitons in Single-Walled Carbon Nanotubes. *Nano Lett.* **2005**, *5*, 2310–2313.
32. Böhmler, M.; Hartmann, N.; Georgi, C.; Hennrich, F.; Green, A. A.; Hersam, M. C.; Hartschuh, A. Enhancing and Redirecting Carbon Nanotube Photoluminescence by an Optical Antenna. *Opt. Express* **2010**, *18*, 16443–16521.